Induction and Repair of DNA DSB as Revealed by H2AX Phosphorylation Foci in Human Fibroblasts Exposed to Low- and High-LET Radiation: Relationship with Early and Delayed Reproductive Cell Death

F. Antonelli,[a,1] A. Campa,[a,b,2] G. Esposito,[a,b] P. Giardullo,[a,c] M. Belli,[b] V. Dini,[a,b] S. Meschini,[a] G. Simone,[a] E. Sorrentino,[a] S. Gerardi,[d] G. A. P. Cirrone[e] and M. A. Tabocchini[a,b]

[a] *Health and Technology Department, Istituto Superiore di Sanità, Roma, Italy;* [b] *National Institute of Nuclear Physics (INFN), Sezione di Roma1, Gr. Coll. Sanità, Roma, Italy;* [c] *Department of Radiation Physics, Università degli Studi Guglielmo Marconi, Rome, Italy;* [d] *INFN-Laboratori Nazionali di Legnaro, Legnaro (Padova), Italy; and* [e] *INFN-Laboratori Nazionali del Sud, Catania, Italy*

Antonelli, F., Campa, A., Esposito, G., Giardullo, P., Belli, M., Dini, V., Meschini, S., Simone, G., Sorrentino, E., Gerardi, S., Cirrone, G. A. P. and Tabocchini, M. A. Induction and Repair of DNA DSB as Revealed by H2AX Phosphorylation Foci in Human Fibroblasts Exposed to Low- and High-LET Radiation: Relationship with Early and Delayed Reproductive Cell Death. ***Radiat. Res.*** **183, 000–000 (2015).**

The spatial distribution of radiation-induced DNA breaks within the cell nucleus depends on radiation quality in terms of energy deposition pattern. It is generally assumed that the higher the radiation linear energy transfer (LET), the greater the DNA damage complexity. Using a combined experimental and theoretical approach, we examined the phosphorylation-dephosphorylation kinetics of radiation-induced γ-H2AX foci, size distribution and 3D focus morphology, and the relationship between DNA damage and cellular end points (i.e., cell killing and lethal mutations) after exposure to gamma rays, protons, carbon ions and alpha particles. Our results showed that the maximum number of foci are reached 30 min postirradiation for all radiation types. However, the number of foci after 0.5 Gy of each radiation type was different with gamma rays, protons, carbon ions and alpha particles inducing 12.64 ± 0.25, 10.11 ± 0.40, 8.84 ± 0.56 and 4.80 ± 0.35 foci, respectively, which indicated a clear influence of the track structure and fluence on the numbers of foci induced after a dose of 0.5 Gy for each radiation type. The γ-H2AX foci persistence was also dependent on radiation quality, i.e., the higher the LET, the longer the foci persisted in the cell nucleus. The γ-H2AX time course was compared with cell killing and lethal mutation and the results highlighted a correlation between cellular end points and the duration of γ-H2AX foci persistence. A model was developed to evaluate the probability that multiple DSBs reside in the same gamma-ray focus and such probability was found to be negligible for doses lower than 1 Gy. Our model provides evidence that the DSBs inside complex foci, such as those induced by alpha particles, are not processed independently or with the same time constant. The combination of experimental, theoretical and simulation data supports the hypothesis of an interdependent processing of closely associated DSBs, possibly associated with a diminished correct repair capability, which affects cell killing and lethal mutation.

INTRODUCTION

One of the most important types of damage induced by ionizing radiation traversing living cells is DNA damage in the context of chromatin, a complex and highly regulated protein–DNA structure. Among the many types of radiation-induced DNA damage, double-strand breaks (DSBs) are considered the most serious lesions in the nucleus, since they are particularly difficult for the cell to repair. Unrepaired or misrepaired DSBs cause mutations or loss of chromosome regions, eventually leading to cell death or neoplastic transformation (*1, 2*).

DSBs may frequently have other associated lesions, such as base-damage and single-strand breaks, and the close location of the lesions to each other is thought to affect their reparability (*3, 4*). Track structure studies indicate that the degree of lesion clustering is dependent on radiation quality. That is, the higher the ionization density at the submicrometric level, the more clustered the damage induced in the double strand of DNA (*5, 6*).

Experimental quantification of the number and distribution of radiation-induced DSBs remains a complex problem, especially at low doses. Techniques such as low-speed sedimentation, constant and pulsed field gel electrophoresis (CFGE and PFGE) (*7, 8*), elution in nondenaturing conditions (*9*) and comet assay (*10*) have been used in the past to study the number of DSBs induced by radiation of

[1] Current address: Laboratory of Radiation Biology and Biomedicine, Agenzia Nazionale per le Nuove Tecnologie, l'Energia e lo Sviluppo Economico Sostenibile (ENEA), Casaccia Research Center, Roma, Italy.

[2] Address for correspondence: Health and Technology Department, Istituto Superiore di Sanità, Viale Regina Elena 299, 00161 Roma, Italy; e-mail: campa@iss.infn.it.

differing qualities [see ref. (*11*) for a review] and its dependence on the repair time (*12, 13*). In particular, PFGE has also been used to detect the DNA fragment mass distribution that is related to the statistical spatial distribution of DSBs (*12, 14*). However, the sensitivity of these approaches is generally not sufficient for detecting DSBs at doses used for detecting cell end points such as cell death and mutation induction, which in general is of the order of few Gy or lower. A significant improvement was made by Rogakou *et al.* (*15*), which utilizes an immunofluorescence technique, which provided the ability to detect even a single DSB per cell. This approach is based on the serine 139 phosphorylation of many molecules (up to 2,000) of histone H2AX (γ-H2AX) after DSB induction in the DNA (*16*). DSBs can be visualized as foci by immunofluorescence using specific antibodies (for γ-H2AX or other proteins involved in DSB repair, e.g., 53BP1), so that enumeration of foci has been used to measure DSB induction and processing after ionizing radiation exposure (*17, 18*). This is currently the only assay that allows the study of DSBs induced in cells by relatively low doses of radiation, i.e. $\leq$1 Gy, and even as low as a few mGy in certain cases (*19, 20*), a value that corresponds, for gamma rays, to an average of one focus for every few tens of cells (*17*).

This technique has been used in the last few years to investigate DSB induction after cells are exposed to low doses of low- and high-linear energy transfer (LET) radiation (*19, 21*), their repair kinetics (*22, 23*) and mechanisms analyzing enzyme co-localization at the DSB site (*24–26*). In general, the number of γ-H2AX foci is found to increase with postirradiation time reaching a broad maximum after about 30 min, and then decrease with a halftime of the order of hours. The phosphorylation-dephosphorylation kinetics depends on several factors including radiation quality (*18, 26, 27*).

As an alternative to the usual observation of foci formed by tracks impinging orthogonally on the cell, some published studies have demonstrated the ability to detect and study γ-H2AX foci formation along a particle track (*27, 28*). Jakob *et al.* (*28*) first reported the distribution of foci along heavy-ion trajectories using irradiation geometry, with the beam directed at a very small angle (below 5°) with respect to the plane of the cell monolayer. Aten *et al.* (*29*) reported that the position of chromosome domains containing alpha-induced γ-H2AX foci are not necessarily fixed and can move to cluster together. This hypothesis is in contrast with the findings of Jakob *et al.* (*30*) who reported that no major motion of damaged chromatin sites exceeding 0.5 μm was detectable within the first minute postirradiation and that for longer amounts of time the migration of DNA lesions seems rather to be a diffusion-like process than an active driven one.

Costes *et al.* (*31*) showed, using high-resolution 3D images, that radiation quality affects both the size and frequency of foci, suggesting that multiple DSBs induced by high-LET nitrogen ions are encompassed within large nuclear domains of 4.4 Mbp, compared with the 1.8 Mbp nuclear domain relative to gamma-ray-induced foci.

Although it is commonly assumed that at least for low-LET radiation, there is a direct correlation between γ-H2AX foci and the presence of radiation-induced DSBs, this relationship is not yet completely clear. While studies with human fibroblasts showed a direct correlation between them (*17, 19*) no such correlation was observed in other cell lines, suggesting the presence in these cells of different amounts of endogenous foci that may be due to DSB-related as well as DSB-unrelated mechanisms (*32, 33*). In addition to the cell line difference, it is possible that the discrepancies reported among various studies are due in large part to the lack of an objective and commonly accepted method to identify each individual γ-H2AX focus, i.e., to distinguish it from the background (*34*).

However, there is the additional question of whether the time course of γ-H2AX foci can be used as a marker of DSB repair kinetics. Contradicting data have been reported since the first studies on the subject, that demonstrated that these foci may persist even after DSB rejoining (*35*). In our previous work (*22*), we reported on a DSB rejoining halftime of $\sim$12 min after γ irradiation, studied by using PFGE, which is much faster than the kinetics of γ-H2AX foci disappearance (more than 1 h).

In agreement with these results, it is suggested (*23, 36*) that other events in addition to break rejoining are necessary to cause the loss of γ-H2AX. It has also been suggested that a single persistent focus did not necessarily represent one DSB, but may, e.g., indicate an aberrant chromatin structure due to illegitimate rejoining (*37*) or an altered organization of the chromatin leading to heritable altered phenotypes (*38*). A correlation between γ-H2AX foci loss halftime and surviving fraction for cultured cells has also been proposed (*23*), although there is no general agreement on this hypothesis (*39*).

Radiation quality can be a potential probe to shed light on this topic, since it has been shown to modulate the clustering/complexity and consequently the reparability of radiation-induced DSBs. However, these studies also have the problem that at very high-LET radiation multiple DSBs can be scored as a single focus because they are located so closely together that they induce overlapping phosphorylation sites. It should also be noted that when the observation is made in the same direction of the particle track, it is impossible to distinguish individual sources of fluorescent signals if their axial distance is less than 500–800 nm given the depth resolution limits for objective lenses of the highest numerical apertures available (*40*). Despite these limitations, this irradiation geometry is frequently adopted in many experiments since it involves rather widespread instrumentation and geometry similar to that used for cell inactivation and other end points.

In this work we report on the H2AX phosphorylation-dephosphorylation kinetics after irradiation of human fibroblasts with gamma rays, protons, alpha particles and

carbon ions obtained by fluorescent microscopy with the above mentioned observation geometry. The maximum number of foci, occurring at 30 min postirradiation for each radiation type is highest after gamma irradiation and decreases with increasing LET. Samples irradiated with gamma rays and alpha particles were also analyzed using a confocal microscope with the aim of studying the γ-H2AX foci morphology and evaluating their size distribution after gamma-ray or alpha-particle irradiation.

Moreover, the γ-H2AX disappearance time course was compared with cell killing and lethal mutation, the latter end point being evaluated by delayed reproductive cell death, a phenomenon represented by the reduction in clonogenic potential of the progeny of cells that survive radiation exposure. The results after irradiation with gamma rays, carbon ions and alpha particles highlighted a correlation between these cellular end points and the γ-H2AX foci persistence time.

This article also contains an Appendix section to aid in the interpretation of the experimental data. A model was developed with the purpose to evaluate, in combination with the experimental data, the probability that multiple DSBs reside in the same gamma-ray-induced γ-H2AX focus. Our calculations show that this probability is extremely low for doses lower than 1 Gy. We have also provided evidence that the DSBs located inside complex foci (i.e., foci with multiple DSBs), such as those induced by alpha particles, are not processed independently. Moreover, the combination of experimental and simulation data support the hypothesis of a nonindependent processing of closely located DSBs, possibly associated with a diminished correct repair capability.

MATERIALS AND METHODS

Cell Culture

Primary human foreskin fibroblasts (AG01522 cell line) were obtained from the Genetic Cell Repository at the Coriell Institute for Medical Research (Camden, NJ). Cells were grown in a monolayer at 37°C, in humidified air supplemented with 5% CO_2, in alpha-minimum essential medium containing 1 m*M* glutamine and supplemented with 20% fetal bovine serum (FBS), 2% HEPES buffer solution (1 *M*), 50 U/dm^3 of penicillin and streptomycin (all reagents from Gibco®-Invitrogen, Grand Island, NY), with a doubling time of ~24 h. All experiments were performed with cells at passage 9–14, in G_0/G_1 phase.

For γ-H2AX foci analysis, AG01522 cells from a confluent flask were trypsinized and plated at a density of 2.1×10^4 cells/cm^2, 14–16 h before irradiation. With this protocol we were able to minimize the presence of cells in the S phase of the cell cycle, as confirmed by flow cytometry measurements (data not shown). For cell killing experiments, AG01522 cells were plated at the same density as γ-H2AX experiments in T-25 flasks or in specially designed petri dishes, depending on the radiation type used.

Irradiation

Irradiation with gamma rays or alpha particles was performed at the Istituto Superiore di Sanità (ISS, Rome, Italy) using γ rays from a ^{137}Cs source, dose rate ≈1 Gy/min (Gammacell® 40, Nordion Inc., Ottawa, Canada) or an alpha-particle irradiator equipped with the ^{241}Am source (total activity: 3.7 MBq) developed at the ISS (*41*). At the cell entrance the alpha-particle energy was 0.75 MeV/u, with LET = 125.2 keV/μm and dose rate ≈0.08 Gy/min. All LET values in this work are calculated in MS20 tissue. Proton irradiation was performed at the Van de Graaf CN accelerator of the Laboratori Nazionali di Legnaro of the National Institute of Nuclear Physics (INFN, Padova, Italy). Proton energy at the cell entrance was 0.84 MeV corresponding to a LET value of ~28.5 keV/μm. Carbon-ion irradiation was performed at the CATANA facility of the Laboratori Nazionali del Sud of the INFN (Catania, Italy), using a 58 MeV/u carbon-ion beam corresponding to a LET value of ~39 keV/μm at the cell entrance.

For gamma irradiation, AG01522 cells were plated on T-75 flasks for cell killing experiments and on slide flasks, cover slips or Mylar® foils for γ-H2AX foci analysis. Previous experiments indicated no differences in γ-H2AX foci induction when cells were seeded on glass or Mylar (data not shown).

Specially designed petri dishes were used for all charged particle irradiations. In particular, cells exposed to protons or carbon ions were plated in stainless steel cylinders (13 mm in diameter) with a Mylar bottom of 52 μm thickness (*42*). For alpha-particle experiments, the petri dish was a stainless steel cylinder with a 56 mm inner diameter, corresponding to an area of 24.6 cm^2 (i.e., comparable to the commercial T-25 flask used for gamma irradiation) and a 3 μm thick Mylar bottom (*41*).

Immunofluorescence for γ-H2AX Foci Detection

Cells were irradiated at room temperature in culture medium, which was replaced with warm medium (37°C) immediately after irradiation. The cells were then incubated at 37°C for different times, up to 24 h, before processing to analyze the phosphorylation-dephosphorylation kinetics. After the required postirradiation incubation times, cells were fixed with 2% paraformaldehyde in phosphate buffered saline (PBS) for 10 min at 4°C, washed three times with PBS and permeabilized with cold methanol for 5 min. Cells were then blocked for incubated with mouse monoclonal anti-γ-H2AX antibody (Upstate®, Millipore, Billerica, MA) at 1:400 dilution for 2 h at 37°C. Cells were washed three times with 0.05% Tween® 20 in PBS and incubated with Alexa Fluor® 488-conjugated goat anti-mouse secondary antibody (Invitrogen™, Carlsbad, CA) at 1:500 dilution for 1 h at room temperature. Cells on cover slips or on Mylar foils were washed four times in PBS and 0.05% Tween 20 for 10 min and mounted using Vectashield® mounting medium with DAPI (Vector Laboratories, Burlingame, CA). Fluorescence images were captured using a Leica Fluorescence Microscope (Leica Microsystems Inc., Wetzlar, Germany). γ-H2AX foci were counted by eye using a 100× immersion objective. The threshold adopted to accept a bright spot as a γ-H2AX focus is purely subjective and it has been fixed around 0.29 μm^2. Statistical analysis was performed on data obtained from at least three independent experiments.

Three-dimensional reconstructed images obtained by confocal microscopy were used to analyze γ-H2AX foci induced by gamma rays or alpha particles. Cell nuclei were stained with propidium iodide. A Leica TCS SP2 spectral confocal microscope (Leica Microsystems), equipped with argon and helium-neon lasers, was used and images were processed using the LCS (Leica Microsystems) software program.

Early and Delayed Reproductive Cell Death

Early and delayed reproductive cell death were measured using the colony-forming assay. Here, ''early'' refers to the classic clonogenic survival, while ''delayed'' reproductive cell death represents the reduction in clonogenic potential of the progeny of cells that survive radiation exposure, i.e., the occurrence of lethal mutations. It is generally thought that this effect, transmissible over many generations, is due to induced genomic instability in the cell population (*43, 44*).

Briefly, after irradiation cells were trypsinized, counted, diluted and plated into four T-75 flasks at the appropriate concentration to score a number of colonies ranging from 300–600 for each dose. After about 12 days of growth at 37°C, viable clones from three flasks were fixed, stained and scored for early survival evaluation (colonies with more than 50 cells were considered as survivors). The fourth flask was trypsinized and cells plated and left for an additional 12 days of growth at 37°C before staining and scoring for delayed reproductive cell death evaluation.

The plating efficiency (*PE*) in control cells was about 20%. Dose-response curves were obtained for both early (cell killing) and delayed (lethal mutations) cell death. For each experiment, cell surviving fractions [*S*(*D*)] were calculated as the ratio between the measured plating efficiency at dose (*D*), *PE*(*D*), and the extrapolated plating efficiency to 0 Gy, $PE(0)_{extr}$. This was evaluated by fitting the function:

$$PE(D) = PE(0)_{extr}\exp(-\alpha D - \beta D^2)$$

to the experimental plating efficiencies measured at the various doses (including $D = 0$ Gy). For all radiation types, beta was not statistically significant so that the fitting procedure was performed with alpha as the only free parameter besides $PE(0)_{extr}$. Cell surviving fractions $S(D) = PE(D)/PE(0)_{extr}$ at each dose were evaluated as the mean from at least three independent experiments with its standard error and the linear parameter alpha was determined by the best fit of the equation: $S(D) = exp(-\alpha D)$.

THEORETICAL EVALUATION OF γ-H2AX FOCI NUMBER IN CELLS WITH RANDOMLY INDUCED DSBs

The phosphorylation of H2AX molecules involves a large DNA region, which in genomic distance extends for a length of the order of the megabase pairs (Mbp), and therefore it is possible that a single γ-H2AX focus is associated with more than one DSB (*31*). This is especially important for DSB induction by charged particles, since it is expected that clustered damage, in particular two or several closely associted DSBs (in genomic as well as in physical space), occur with high frequency. Therefore, the number of foci is seldom equal to the number of radiation-induced DSBs. Evaluation of the probability of having more than one DSB associated to a given focus after charged particle irradiation depends mainly on what is known about the spatial correlation between DSBs induced by a single track. After gamma irradiation, it is reasonable to perform an analysis assuming that DSBs are randomly induced. If the distance between DSBs is defined in terms of genomic distance, then one can use the broken stick model (*45–48*) to compute the average number of ''visible'' DSBs, i.e., the average number of distinct foci. The computations are described in the Appendix section and here we give the final result. We assume that cells are irradiated with a dose (*D*), and we are interested in the average number of induced DSBs that, in a chromosome of genomic length (*L*), are at a genomic distance not smaller than x_1, taken as the minimum distance between DSBs that gives rise to distinct visible foci. Denoting the lengths by the corresponding masses, $x_1 \to M_1$ and $L \to M$, we derive the following expression for the average number of distinct foci $\langle s\rangle_{M_1,D,M}$, due to DSBs induced by a dose (*D*) on a chromosome of length (*M*) and at distances greater than M_1:

$$\langle s\rangle_{M_1,D,M} = [Dy(M - M_1) - 1]e^{-DyM_1} + 1 \qquad (1)$$

We have applied this expression to our results concerning γ irradiation, taking into account the lengths of the chromosomes in a human cell. Here we just state that the values of the right-hand side in the two limits are $M_1 \to 0$ and $M_1 \to M$, respectively. In the former case we recover the average number of radiation-induced DSBs, i.e., *DyM*, while in the latter we have the probability to induce at least one DSB, i.e., $1 - e^{-DyM}$.

For charged particle irradiation one may consider another limiting situation, which actually seems to occur in our data (see Results). This is the case in which no particle track can give rise to more than a distinct focus. Practically this means that, no matter how many DSBs are induced by the passage of a given track (provided that at least one is induced), only one focus will be resolved. This is what happens for our irradiation geometry, with the particle beam impinging perpendicularly on the cell layer. Then the number of detected radiation-induced foci in a given cell corresponds to the number of tracks inducing at least one DSB.

The average number of tracks traversing a cell nucleus, $\langle q\rangle$, can be evaluated when the dose, the LET and the nucleus area are known. If we denote by p_0 the probability that a given track does not induce any DSB, then we expect that the average number of detected radiation-induced foci are given by $\langle q\rangle$ $(1 - p_0)$. Thus, measuring the average number of detected foci gives an estimate of p_0. On the other hand, if $\langle m\rangle$ is the average number of DSBs induced by a single track, the average number of DSBs in a nucleus will be equal to $\langle q\rangle\langle m\rangle$. If this number is evaluated by the DSB yield of the given radiation, we obtain an estimate of $\langle m\rangle$. We note that an evaluation of both $\langle m\rangle$ and p_0 gives an indication of the DSB correlation along a particle track. In fact, for uncorrelated DSBs we would expect $p_0 = e^{-\langle m\rangle}$, while we can argue that with a positive DSB correlation (i.e., if the occurrence of one DSB increases the probability of occurrence of another DSB close by) p_0 and $\langle m\rangle$ will not be related in this way.

STATISTICAL ANALYSIS OF THE γ-H2AX DEPHOSPHORYLATION KINETICS

Although the H2AX phosphorylation maximum occurs 30 min after exposure for all radiation types, as shown in the Results, the behavior of the dephosphorylation curve is different between gamma rays and charged particles. In particular the γ-H2AX foci dephosphorylation is slower for charged particles than for gamma rays. This difference can be quantified considering the cumulative probability distribution function for the foci disappearance. Let us denote by $f(t)$ the probability distribution function for the disappearance time of a visible focus, such that $f(t)dt$ is the probability that a focus disappears between t and $t + dt$. The

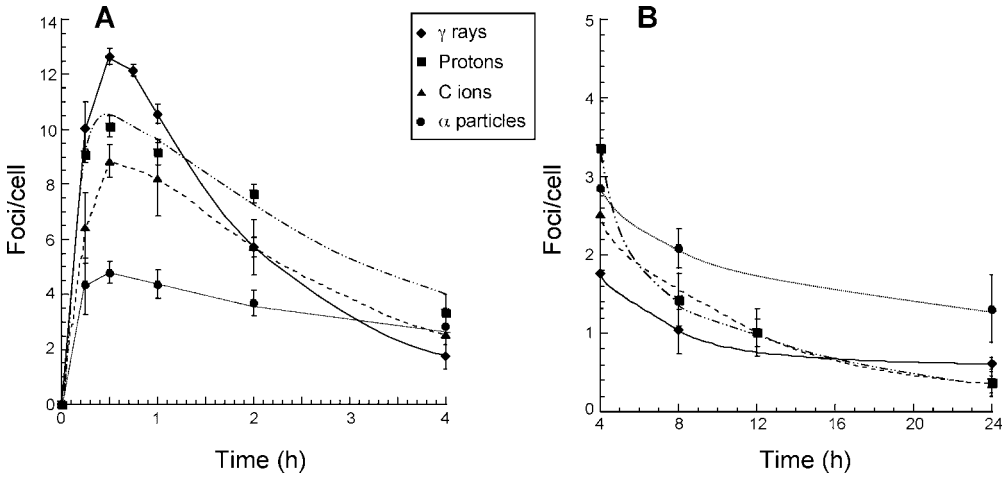

FIG. 1. Phosphorylation-dephosphorylation kinetics of H2AX foci induced in AG01522 cells after irradiation with 0.5 Gy of γ rays (solid diamond), protons (solid square), carbon ions (solid triangle) and alpha particles (solid circle). H2AX kinetics are reported up to 4 h (panel A) and from 4–24 h (panel B) after irradiation. At least eight independent experiments were performed for γ rays, five for protons, four for carbon ions and seven for α particles. Net data are reported, after subtraction of the control values. The error bars represent the standard error of the mean.

probability that a focus has disappeared before a given time (t) after the beginning of the dephosphorylation (at time t_0) is given by the cumulative distribution function $F(t)$:

$$F(t) = \int_{t_0}^{t} f(t')\,dt' \tag{2}$$

This definition implies that $f(t)$ is different from 0 only for $t \geq t_0$, and that it is normalized so that $F(\infty) = 1$. The cumulative distribution function was determined for gamma rays, alpha particles, carbon ions and protons starting from the experimental data of the mean number of foci N_f. For this purpose the beginning time of the dephosphorylation, t_0, was assumed to be equal to 30 min and the mean number of foci at $t > 30$ min was normalized with respect to that at t_0, i.e., $N_f(t)/N_f(t_0)$. This ratio is the probability that a visible focus is still there at the given time (t). Then, the probability that a visible focus disappears before t, i.e., the experimental cumulative distribution function $F_{exp}(t)$, is given by $1 - [N_f(t)/N_f(t_0)]$.

A possible theoretical approach to investigate how clustered DSBs can affect foci disappearance is to make the working hypothesis that the m DSBs constituting a complex focus are independently processed by the repair enzymes and that all of these DSBs must be repaired before the focus disappears. With these assumptions, the cumulative distribution function $F_m(t)$ for foci with a given fixed number m of DSBs is simply related to the cumulative distribution function $F_1(t)$ for simple foci with only one DSB:

$$F_m(t) = F_1^m(t), \tag{3}$$

that is, $F_m(t)$ is the mth power of $F_1(t)$. A more realistic case is that the number m of DSBs in the charged particle complex focus is distributed according to a given probability distribution $P(m)$. In this case the cumulative distribution function $F_c(t)$ for charged particles becomes:

$$F_c(t) = \sum_m P(m) F_1^m(t) \tag{4}$$

RESULTS

H2AX Phosphorylation-Dephosphorylation Kinetics as a Function of Radiation Quality

The kinetics of phosphorylation and dephosphorylation of γ-H2AX in AG01522 cells after a dose of 0.5 Gy of gamma rays indicates that the maximum number of radiation-induced foci (i.e., the number of foci net of the corresponding control value) is 12.64 ± 0.25 and that it is reached 30 min after irradiation (Fig. 1A). This time is in agreement with previous findings (*21, 22, 24*). Based on data from the literature, a correlation (one to one) is expected between the number of DSBs that are located at a distance greater than 2 Mbp and the number of γ-H2AX foci. To verify this correlation, we calculated the expected number of DSBs located at a distance greater than 2 Mbp for 0.5 Gy of gamma rays using Eq. (1) obtained by the broken stick distribution. In this calculation we considered the single chromosomes of the human male karyotype and a yield (y) of $6.29 \cdot 10^{-3}$ $Mbp^{-1}Gy^{-1}$, obtained by PFGE analysis (*49*). The results showed that for this value of D and y the number of DSBs that are located at a distance greater than 2 Mbp is 18.6, while the total number of DSBs is 18.7, indicating that the gamma-ray-induced DSBs should almost entirely be located at genomic distances greater than 2 Mbp. The difference of these calculated values from the experi-

TABLE 1
Persistence Ratio of γ-H2AX Foci after Exposure to Different Radiation Qualities

Radiation type	2 h	4 h	8 h	12 h	24 h
γ rays (^{137}Cs)	45.19	13.90	8.22		2.53
28.5 keV/μm protons	75.91	33.21	14.16	9.97	3.72
39.4 keV/μm C ions	64.58	28.47		11.43	3.98
125 keV/μm α particles	76.79	59.19	43.34		27.29

mental number of 12.64 indicated above, obtained for 0.5 Gy radiation-induced γ-H2AX foci, could be related to an overestimation of PFGE data, due to the conversion of heat-labile sites to DSBs during lysis in the PFGE experiments used to measure the DSB yield (*50, 51*) (see Discussion).

Figure 1 also shows a comparison of the gamma-ray-induced phosphorylation/dephosphorylation kinetics of γ-H2AX with those obtained after irradiation of AG01522 cells with 0.5 Gy of protons, carbon ions or alpha particles. For better visualization we have divided the time course of the phosphorylation/dephosphorylation kinetics between Fig. 1A (up to 4 h) and Fig. 1B (from 4–24 h). Differences in the number of foci are evident as early as 15 min. The maximum number of foci is reached 30 min postirradiation for all the radiation types, but the number of foci induced are different namely, 10.11 ± 0.40, 8.84 ± 0.56 and 4.80 ± 0.35 for protons, carbon ions or alpha particles, respectively.

In addition, the phosphorylation-dephosphorylation kinetics are clearly different. To make comparisons on a quantitative basis, we introduced a parameter able to quantify the foci persistence into the cell, the persistence ratio (PR), defined as the percentage of the number of radiation-induced foci at the time (t) with respect to the maximum number of radiation-induced foci (obtained at 30 min), for the same radiation type. PR values relative to all radiation types used are shown in Table 1. The values calculated using different amounts of time after radiation exposure indicated that the γ-H2AX foci persistence is dependent on radiation quality: the higher the LET, the longer the foci persist in the cell nucleus. To explain this finding, particularly significant for alpha particles, two different potential scenarios are possible: 1. That an alpha-induced focus could contain more than one DSB; 2. That the high-LET-induced DSBs are more complex and consequently more difficult for the cell to repair than the gamma-ray-induced DSBs.

We compared the number of tracks calculated and measured by using CR39 dosimeters with the number of γ-H2AX foci induced in the cell nucleus by the radiation with the highest LET, namely alpha particles (LET: 125.2 keV/μm). The average area of AG01522 cell nuclei was about 210 ± 20 μm^2, as measured by fluorescent microscopy using DAPI as nuclear dye for approximately 200 cells. This value has been used to calculate the average number of tracks produced by 0.5 Gy alpha-particle irradiation in a cell nucleus. In fact, from the dose (D) and the LET values, the fluence (F) can be computed from the equation

$$D = 0.16\,\frac{F{\cdot}LET}{\rho}, \qquad (5)$$

where dose is expressed in Gy, the fluence in μm^{-2}, the LET in keV/μm and the density (ρ) in g/cm^3. A dose of 0.5 Gy of alpha particles corresponds to a fluence of 0.025 particles/μm^2. Therefore, the average number of tracks/nucleus obtained is 5.25 ± 0.50, in very good agreement with the average number of tracks measured by CR39 dosimeters, which was 5.23 ± 0.50. The number of tracks is also very similar to the counted maximum number of foci (4.80 ± 0.45). Actually, we expect that each alpha particle would produce several DSBs. The average number of DSBs per track could be evaluated by knowing the delivered dose and the DSB yield. Not having our own experimental data from PFGE analysis, we resorted to evaluations obtained by simulations with the PARTRAC Monte Carlo code [for information on the structure and properties of the PARTRAC code see refs. (*14, 52*)], considering human fibroblasts irradiated with 0.5 Gy of alpha particles (Alloni, personal communication). Simulations gave an average of 8 DSBs per track, with about half of them at genomic distances within a few tens of kbp. Accordingly, we assume that each focus, observed orthogonally to the cell surface, corresponds to an average of 8 DSBs.

Statistical Analysis of the γ-H2AX Dephosphorylation Kinetics

In Fig. 2 we show the experimental cumulative distribution function $F_{exp}(t)$, previously defined, related to the dephosphorylation kinetics. In particular, in each panel we compare the kinetics after gamma irradiation with the kinetics after irradiation with charged particles: alpha particles (Fig. 2A), carbon ions (Fig. 2B) and protons (Fig. 2C). In the plots the variable x is defined by $x = t - t_0$, where $t_0 = 0.5$ h is the time of maximum phosphorylation, with the time (t) taking the values $t = 1$, 2, 4, 8 and 24 h. In all cases the probability of foci disappearance for gamma irradiation is greater than for charged particle irradiation, and the largest difference occurs for alpha particles. In the spirit of the approach mentioned above, and assuming that the slower repair kinetics observed is due to the greater complexity of the foci induced by charged particles (i.e., the larger number of DSBs inside a single focus), or to multiple DSBs in the same track, we have compared the experimental distributions to the theoretical distributions defined by Eqs. (3) and (4), with $F_1(t)$ given by the experimental distribution after gamma irradiation. This procedure rests on the assumption that, for doses lower than 1 Gy, the probability to have more than one DSB in a gamma-ray-induced focus is negligible. This assumption, as shown in the previous section, has been given solid quantitative

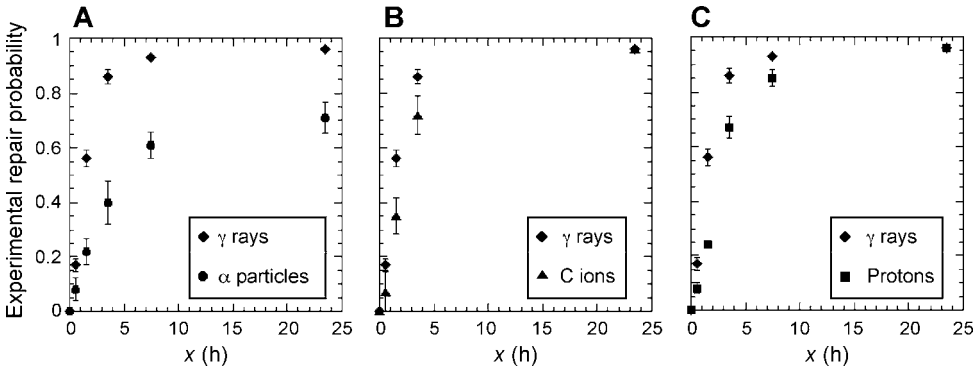

FIG. 2. Experimental cumulative distribution function $F(x)$ for γ rays (solid diamond), panel A: alpha particles (solid circle), panel B: carbon ions (solid triangle) and panel C: protons (solid square). The variable x is equal to t – 0.5 h. For carbon ions the point corresponding to $t = 8$ h is missing.

justification. On the contrary we assume that for alpha particles, carbon ions and protons a focus can be a complex focus composed of several DSBs. In the simple model presented above, the experimental distribution after charged particle irradiation can be compared to the theoretical one, shown in Eq. (3), choosing the value of m that gives the best agreement; clearly this optimal m value depends on the type of charged particle. In the more complex model, represented by Eq. (4), one optimizes the parameters of the probability distribution $P(m)$. In the case of the simple model, using Eq. (3), the best results correspond to $m = 7$ for alpha particles and to $m = 2$ for both carbon ions and protons (data not shown). At long repair times ($t \geq 8.5$ h) the presence of 7 DSBs/track fits quite well with the alpha-particle experimental results. On the other hand, at shorter repair times the agreement is not good, and the experimental probability is better reproduced by a smaller number m of DSBs per focus. Additionally, for carbon ions and protons, the agreement is not very good. In the more realistic case where the number m of DSBs along the particle tracks is distributed according to a given probability distribution $P(m)$ the theoretical cumulative distribution function $F_c(t)$ is defined in Eq. (4). For example assuming that the number m of DSBs/track is distributed according to the Poisson distribution $[P(m,\langle m\rangle) = (\langle m\rangle^m exp(-\langle m\rangle)/m!)]$ the best result is obtained considering a Poisson distribution with mean value $\langle m\rangle = 7$ for alpha particles, $\langle m\rangle = 2.5$ for carbon ions and $\langle m\rangle = 2.9$ for protons, as shown in Fig. 3A, B and C, respectively (again, $x = t - t_0$). At shorter times the agreement between the theoretical and experimental distributions for alpha particles is slightly improved, although in this case it is also not satisfactory. In addition, the agreement for carbon ions and protons remains not good. We have verified that when considering other distributions $P(m)$ in Eq. (4) the agreement between theoretical and experimental cumulative distribution functions for charged particles does not improve meaningfully. As a matter of fact, the assumption of a Poisson distribution of the number of DSBs caused by a charged particle track is not well justified. Also, assuming a Poisson distribution would result in the hypothesis that along the track there is a constant probability per unit length of inducing a DSB independently from the DSBs already induced. However, it can be assumed that in a given track portion immediately after one DSB induction, the proba-

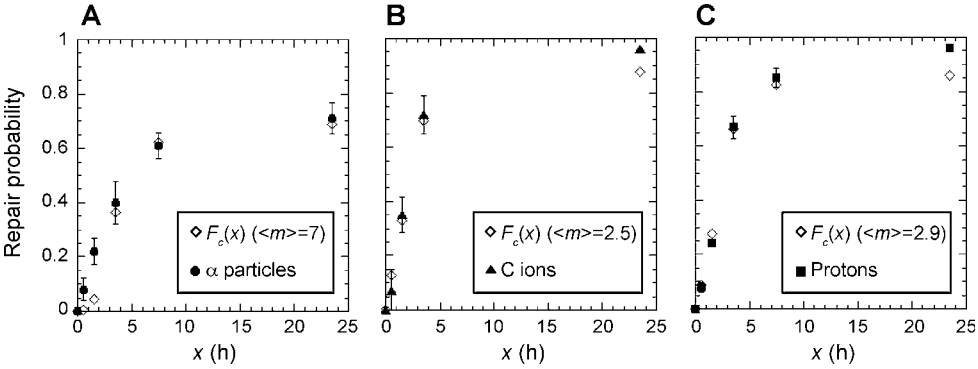

FIG. 3. Comparison between Eq. (4), with $F_1(x)$ given by the experimental distribution function after γ irradiation and $P(n)$ by a Poisson distribution, and the experimental probability distribution after charged particle irradiation: $F_c(x)$ with $\langle m\rangle = 7$ (open diamond) and experimental $F(x)$ for alpha particle (solid circle) (panel A), $F_c(x)$ with $\langle m\rangle = 2.5$ (open diamond) and experimental $F(x)$ for carbon ions (solid triangle) (panel B); and $F_c(x)$ with $\langle m\rangle = 2.9$ (open diamond) and experimental $F(x)$ for protons (solid square) (panel C). The variable x is equal to t – 0.5 h.

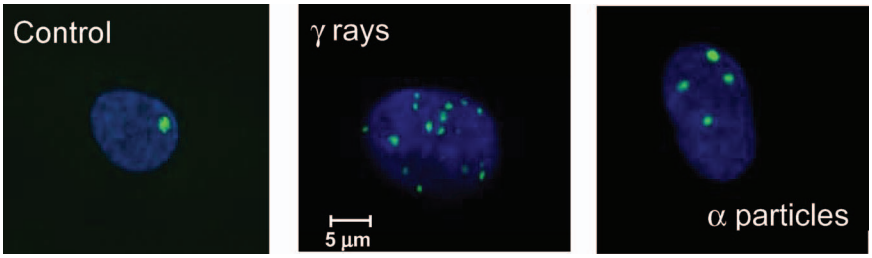

FIG. 4. Representative images of nonirradiated (control) and radiation-induced γ-H2AX foci. Images of radiation-induced γ-H2AX foci refer to samples exposed to 0.5 Gy of γ rays or α particles and incubated for 30 min postirradiation. Fluorescence images were captured using a 100× immersion objective. DAPI was used to stain the nucleus.

bility of inducing an additional DSB is greater than in the same portion in a generic point of the track; this is due to the fact that an induction of a DSB means that the track is traversing a region very close to the DNA double helix. Thus, the real $P(m)$ is not expected to be a Poisson distribution, however, we do not know its form. For this reason we have computed Eq. (4) for several distributions, not only for the Poissonian one; nevertheless, we find that the agreement with the experimental distribution is always unsatisfactory.

This negative result suggests that several DSBs constituting a complex focus along the particle track for alpha particles, carbon ions and protons could be correlated, so that no individual DSB is independently processed by the repair enzymes. There is also, in principle, the possibility that the single DSBs in a complex focus, although processed independently, are each repaired slower than gamma-ray-induced DSBs; this should result in an optimal m such that the comparison with the experimental data would be satisfactory at all times, after a time rescaling. However, we could not verify this possibility. Of course, a combination of the two factors (slower processing of each DSB and correlated processing of the DSBs in a focus) cannot be ruled out.

γ-H2AX Foci Morphology and Size Distribution

Nonirradiated (control) cells were analyzed to evaluate the percentage of cells with γ-H2AX foci as well as foci size. γ-H2AX foci were counted and analyzed in a total of 6,815 AG01522 cells. Foci areas smaller than 0.29 μm^2, as specified in Materials and Methods, were considered as background signals. Our results indicate that about 29.1 ± 0.3% (error has been calculated on the hypothesis that the presence or absence of foci follows a Poissonian distribution) of control cells show γ-H2AX foci and that the average number of foci per cell is 0.48 ± 0.04.

The size distribution of γ-H2AX foci has been analyzed in about 300 nonirradiated cells by conventional fluorescence microscopy. We found an average foci size of 1.84 ± 0.1 μm^2. This value is in very good agreement with the mean value of 1.68 μm^2 reported for ''large foci'' in human fibroblasts by Costes *et al.* (*31*). Moreover, this value is between the gamma-ray- and alpha-particle-induced foci areas (values reported below). Noteworthy is the presence of large foci (~42% of the total number of foci analyzed) after alpha particles compared to the typical gamma-radiation-induced foci. Here we define large foci as those with an area larger than the average value of 1.84 μm^2. A representative image of a nucleus with foci is shown in Fig. 4 for the control case (CN, left panel), gamma-irradiated cells (γ-rays, center panel) and alpha-particle-irradiated cells (α-particles, right panel).

When cells are exposed to high-LET radiation, such as alpha particles, the induced γ-H2AX foci show differences in size and morphology compared to γ ray-induced foci. These differences can be due to several factors, including the different modalities of energy deposition of sparsely and densely ionizing radiation that induce DSBs of different spatial distribution, which in turn can lead to a possible different chromatin fiber relaxation. Moreover, alpha particles can induce several DSBs along a single track, with neighboring double breaks resulting in overlapping foci, a pattern that is highly improbable for gamma rays at the doses used in this work.

To further investigate these differences, a confocal microscopy study was performed on cells incubated for 30 min at 37°C after irradiation with gamma rays or alpha particles. Due to the localized release of energy by alpha particles into the cell nucleus, individual but closely located γ-H2AX foci would be expected to form along the DNA with significant frequency. When the conventional fluorescence microscope was used, it was not possible to distinguish separate γ-H2AX foci along the particle track. Assuming the extension of γ-H2AX phosphorylation of about 2 Mbp along the DNA fiber surrounding the DSB for low-LET-induced foci and about 4 Mbp (*31*) for high-LET-induced foci, the inability to detect more than one focus along the same track could be due to the overlapping of phosphorylation zones relative to different DSBs close to each other and/or to the insufficient resolution of the fluorescent microscope used in this work. Using confocal microscopy, we measured the nucleus thickness after staining with propidium iodide, obtaining a value of about 3 μm. *xy* sections of about 100 gamma- and alpha-induced foci (dose: 0.5 Gy) were taken along the Z axis at intervals

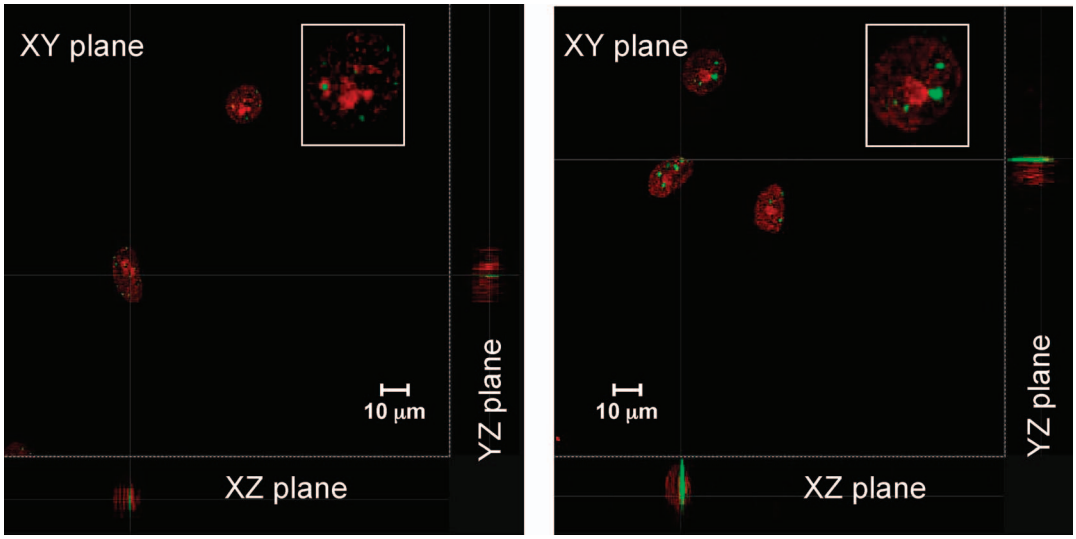

FIG. 5. Two- and three-dimensional visualization of radiation-induced γ-H2AX foci in AG01522 cells after exposure to gamma rays (left panel) or alpha particles (right panel). Foci extension along the X axis is reported on the XZ and YZ planes after 3D reconstruction of confocal section fluorescence. Cell nuclei were stained with propidium iodide (red).

of about 0.2 μm. Representative reconstructions of the fluorescence along the XZ and YZ planes are shown in Fig. 5, where the left panel refers to gamma rays and the right panel to alpha particles. No separate foci could be observed at 30 min after irradiation with either gamma rays or alpha particles, although a substantial difference in track thickness is evident between these two radiation types.

Moreover, the analysis of the size distribution of gamma- and alpha-induced γ-H2AX foci was performed on 3D reconstructed images where about 100 foci were analyzed for both types of radiation. Distribution of γ-H2AX foci areas in nonirradiated cells (from conventional fluorescence microscopy analysis) and in cells irradiated with gamma rays and alpha particles to a dose of 0.5 Gy (from confocal microscopy) are shown in Fig. 6. Radiation-induced γ-H2AX foci size distributions revealed that alpha-particle-induced foci are larger than those induced by gamma rays, being the mean size values of 2.10 ± 0.11 μm^2 and 1.26 ± 0.09 μm^2, respectively. In addition, after irradiation with α particles, about 5% of cells show foci areas larger than 5 μm^2, while no cells show this foci size when irradiated with γ rays.

Dose-Response Curves for DNA DSB Induction

To determine the dose dependence of γ-H2AX foci induction after low- or high-LET exposure, AG01522 cells were irradiated with different doses (up to 1 Gy) of gamma rays or alpha particles. The number of γ-H2AX foci was always determined 30 min after irradiation (time corresponding to the maximum number of γ-H2AX foci induced by gamma rays or alpha particles). As shown in Fig. 7, a linear dose dependence was observed for both low- and high-LET radiation. The dose-response curves were fitted by a linear function with the least-squares method, giving slopes of 24.1 and 8.8 foci per Gy per cell nucleus for gamma rays and alpha particles, respectively. From the slopes of these curves, the relative biological effectiveness (RBE) of alpha particles for DSB induction would appear to be less than 1. This is due to the difference between gamma rays and charged particles in the relationship between DSB induction and γ-H2AX foci production. As we previously mentioned, for alpha particles the number of foci is expected to coincide with the number of tracks, and according to Monte Carlo simulations, each track induces an average of 8 DSBs. Furthermore, we re-emphasize that separate foci are not visible along an alpha-particle track, even with the confocal microscope.

Although we have not performed a confocal microscope study for the γ-H2AX foci produced by protons and by carbon ions, by computing with Eq. (5) the average number of tracks per cell nucleus for a dose $D = 0.5$ Gy, we obtain 16.8 ± 1.6 for carbon ions and 23.1 ± 2.2 for protons. These numbers are larger than the maximum numbers of the observed foci at that dose, which are 8.84 and 10.11, respectively. These data can be reconciled by assuming that a fraction of proton and carbon-ion tracks does not induce any DSBs, and thus does not produce any focus. Monte Carlo simulations performed for carbon-ion irradiation (Alloni, personal communication) confirm this assumption, showing that about 35% of the carbon-ion tracks induce at least 1 DSB. The difference with the observed ratio between the number of foci and the number of tracks ($8.84/16.8 = 0.53$) could be explained assuming that delta rays from some tracks are able to induce DSBs at some distance from the track. As a matter of fact, the maximum range of the delta rays for carbon ions of the energy considered in this work is about 200 μm, i.e., long enough to induce a DSB far

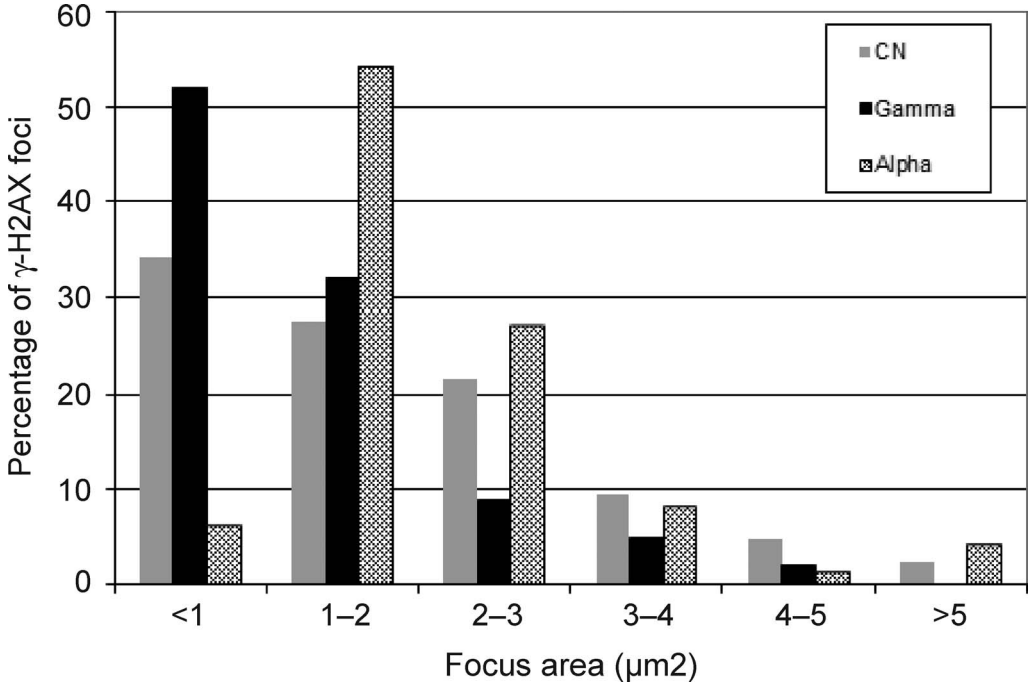

FIG. 6. Distribution of γ-H2AX foci areas in AG01522 cells irradiated with gamma rays (solid bar) or alpha particles (shaded bar) and in control cells (gray bar). A total of 100 foci areas were measured for each radiation type using a 100× immersion objective (confocal microscopy), while a total of 170 foci areas were measured in control cells using a 100× immersion objective (conventional fluorescence microscopy). The average foci size was 1.26 ± 0.09 μm^2 and 2.10 ± 0.11 μm^2 for gamma rays and alpha particles, respectively and 1.84 ± 0.10 μm^2 in control cells.

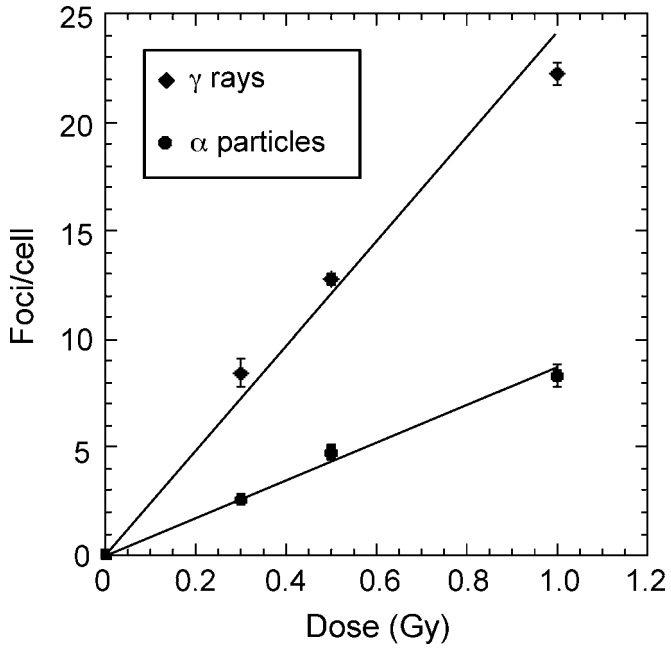

FIG. 7. Average number of γ-H2AX foci/cell induced in AG01522 cells as a function of radiation dose for gamma rays (solid diamond) and alpha particles (solid circle) from at least 3 independent experiments. Foci were quantified following a postirradiation incubation for 30 min at 37°C. The error bars represent SEM values.

from the track, possibly in a nearby cell (while a single cell is simulated in PARTRAC).

Cell Killing and Lethal Mutations

Dose-response curves were obtained for cell killing and lethal mutations (as measured by early and delayed cell death, respectively) in AG01522 cells exposed to different types of radiation. In addition to gamma rays and 125 keV/μm α particles, 39.4 keV/μm carbon ions have been used for these experiments. As shown in Fig. 8 (Fig. 8A refers to early survival and Fig. 8B to late survival), linear relationships have been obtained for all radiation types considered. The best-fit parameters as well as the RBE values are reported in Table 2.

In accordance with their ionization density, charged particles are more effective than gamma rays in inducing cell killing and lethal mutations: in both cases the survival curves for carbon ions and alpha particles show slope values increasing with LET and giving RBE values, evaluated by the α/α_γ ratio, of 1.26 and 2.98 for cell killing, and of 1.61 and 3.74 for lethal mutations, respectively.

DISCUSSION

The aim of this work was to apply a combined experimental and theoretical approach to study the phosphorylation-dephosphorylation kinetics of radiation-induced

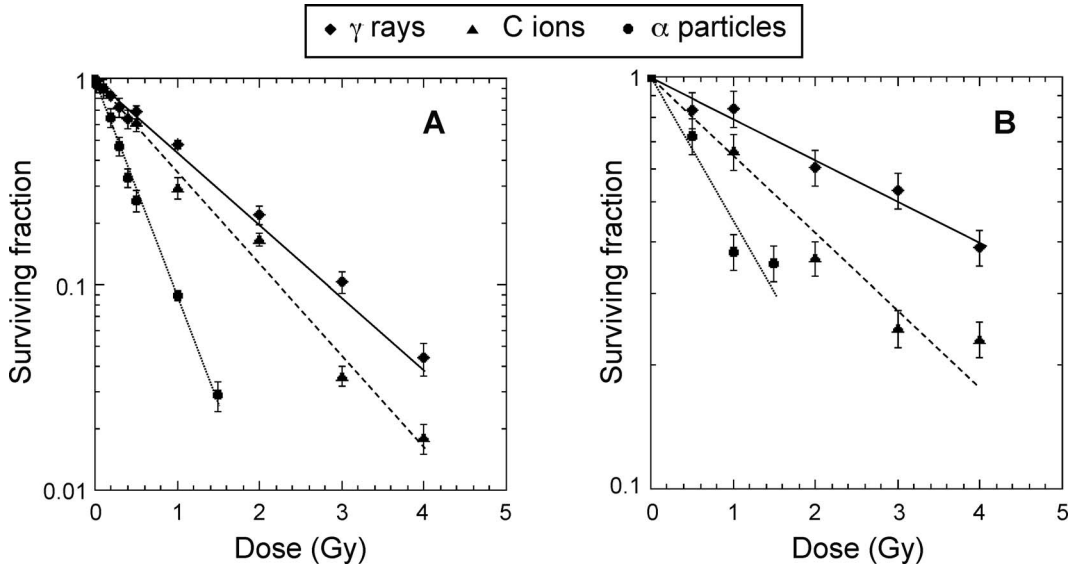

FIG. 8. Dose-response curves for early and late survival of AG01522 primary human fibroblasts irradiated with gamma rays (solid diamond), carbon ions (solid triangle) or alpha particles (solid circle): early survival (panel A), late survival (panel B). Data represent the mean from 3 independent experiments (except those relative to carbon ion and alpha particle late survival that were repeated twice), with its standard error.

γ-H2AX foci, their size distribution and 3D focus morphology, as well as the relationship between DNA damage and cellular end points (i.e., cell killing and lethal mutations). Different radiation qualities, namely gamma rays, protons, carbon ions and alpha particles, were used to clarify the role of the damage complexity in DSB repair by analyzing the persistence of γ-H2AX foci in the cell nucleus.

Analysis showed the presence of γ-H2AX foci in about 30% of unirradiated cells. A significant percentage of these are represented by ''large'' foci with a characteristic morphology and an area between that of gamma-ray-induced foci and that of alpha-particle-induced foci, likely related to physiological DSBs due to senescence (*17*), to permanent changes in the structure of the chromatin fiber and/or to cell cycle arrest mechanisms (*31, 53*).

Despite the considerable advantages of the γ-H2AX assay, primarily associated with the ability to measure low-dose radiation-induced damage through the cellular machinery acting in recognition and processing of DNA DSBs, this assay lacks a standardized procedure for γ-H2AX foci counting. Different size thresholds or approaches (enumeration of γ-H2AX foci by eye or computational methods) are used, sometimes making it difficult to compare data from different laboratories (*34*).

When cells are exposed to ionizing radiation, damage is induced in the DNA, leading to the activation of the repair pathways and checkpoint signaling. In most studies, various DSB repair proteins have been reported to co-localize with γ-H2AX foci (*53, 54*) and mechanisms were proposed for the formation and spread of γ-H2AX as well as for the accumulation/retention of repair proteins at the sites of damage (*55, 56*). A common assumption is that γ-H2AX is a platform for repair protein accumulation and retention and that H2AX phosphorylation is a key process necessary to correct DNA DSB repair (*35*). The foci dephosphorylation process and the precise functions of the residual γ-H2AX, persistent after several hours postirradiation, are less clear.

In this work H2AX phosphorylation-dephosphorylation kinetics were analyzed to evaluate the maximum number of γ-H2AX foci and the persistence of these foci with the time, in an attempt to understand the differences observed after irradiation of AG01522 cells with gamma rays or charged particles of differing quality. We observed the maximum number of γ-H2AX foci after 30 min postirradiation, independent of the radiation type and dose. The γ-H2AX foci yield, determined from the slope of the dose

TABLE 2
Parameters of Survival Curves Shown in Fig. 8 and RBE Values

	Celling killing		Lethal mutations	
Radiation type	α (Gy^{-1}) ± SE	RBE (α/α_γ) ± SE	α (Gy^{-1}) ± SE	RBE (α/α_γ) ± SE
γ rays (^{137}Cs)	0.816 ± 0.023	–	0.231 ± 0.018	–
39.4 keV/μm C ions	1.025 ± 0.021	1.26 ± 0.04	0.373 ± 0.019	1.61 ± 0.15
125 keV/μm α particles	2.432 ± 0.053	2.98 ± 0.11	0.865 ± 0.057	3.74 ± 0.38

SE = standard error.

dependence for gamma irradiation, is 24.1 ± 0.4 foci/Gy/nucleus (assuming a linear dose dependence) (Fig. 7). While this value is lower than that of 36 foci/Gy/cell reported by Rotkamm and Löbrich for MRC-5 primary fibroblasts (*19*), it is in good agreement with the data reported by Costes *et al*. (*31*) and Asaithamby *et al*. (*18*), i.e., 21 foci/cell and 28.6 foci/cell, in HCA2 and HSF42 human fibroblasts, respectively. We can also exclude significant underestimation due to γ-H2AX dephosphorylation within 30 min after irradiation on the basis of our previous studies using calyculin A, a protein phosphatase 1 and 2A inhibitor (*22*).

Moreover, the value of 24.1 ± 0.4 foci/Gy/nucleus as obtained for AG01522 cells is consistent with the yield of 25 DSB/Gy reported some years ago for normal human GM5758 skin fibroblasts by Stenerlöw *et al*. (*50*) and Rydberg (*51*) using a PFGE procedure aimed to avoid the conversion of heat-labile sites to DSBs. Therefore, we can reasonably conclude that a one to one correlation is acceptable for gamma-ray-induced DNA DSBs and γ-H2AX foci, as previously proposed for this type of radiation (*57*). This conclusion is further supported by the results of our theoretical model. Based on the hypothesis of absence of correlation between the DSBs produced by gamma rays, the computation of the probability of having more than one DSB associated to a given gamma-ray-induced focus has been carried out, and the results have shown that for the doses considered, this probability is negligible; this finding allowed us to conclude that the maximum number of gamma-ray-induced γ-H2AX foci at 30 min does not represent an underestimation due to the presence of several DSBs in the same focus. It is worth noting that Ponomarev *et al*. studied the same problem using a different approach. They adopted the strategy to use the Poisson distribution of radiation-induced DSBs in physical space inside the cell nucleus, assigning a volume to a focus and determining the dose-dependent probability that, in the volume associated with a given focus, additional DSBs occur (*58*). Ponomarev *et al*. also showed that for γ irradiation at doses below 1 Gy the probability of having more than one DSB in a focus is negligible.

The decrease in the number of foci observed after charged particle irradiation with increasing LET values may be explained by two effects, both related to radiation quality: 1. Several foci are counted as one focus when they occur along the same track, due to the observation geometry; 2. Several DSBs may occur closely together so that they are included in the same focus. In particular, the first point is confirmed by the confocal microscope images of γ-H2AX foci analyzed along the Z axis. Our observations show that no individual foci can be visualized along the alpha track 30 min postirradiation, in agreement with the data reported by Costes *et al*. (*31*). On the other hand, PARTRAC Monte Carlo code simulations gave an average of 8 DSBs per alpha track, with about half of them at genomic distances within a few tens of kbp. This indicates that, in general, charged particle-induced γ-H2AX foci are related more closely to the number of tracks traversing the cell nucleus than to the number of induced DNA DSBs.

Three-dimensional images of alpha-particle-induced γ-H2AX foci did not help to distinguish individual foci along the trajectory of the particle, in agreement with the findings of Costes *et al*. who analyzed the γ-H2AX foci induced by 32.5 MeV/nucleon nitrogen ions (*31*). The absence of separate foci identified along the same alpha track could also be expected by the resolution limits of the conventional far-field microscopy (500–800 nm). In fact, considering that the AG01522 nuclear thickness is about 3 μm and the average number of DSBs obtained by Monte Carlo simulations is 8, the average distance between them is less than 400 nm, which is smaller than the resolution limit.

The presence of a different quality of induced DSBs is reflected in the different time courses of H2AX phosphorylation-dephosphorylation kinetics obtained after irradiation of AG01522 human primary fibroblasts with charged particles of different quality. Indeed, the same dose induces a different maximum number of γ-H2AX foci 30 min postirradiation with gamma rays, protons, carbon ions or alpha particles. Moreover, with increasing LET, a larger foci persistence is observed: 24 h postirradiation, persistence ratios span from 2.53 for gamma rays to 27.29 for alpha particles.

The association of more than one DSB within a single focus could explain the different kinetics of dephosphorylation observed as could the hypothesis that the DSB are processed independently, and the probabilities to repair each DSB may be affected. Therefore, to ascertain if the different kinetics are due to a different quality of lesion, one must sort out the role of the probability composition. Although we have only shown in a qualitative way by experimental data analysis using a simple model that foci disappearance is driven by independent, same-velocity processing of each DSB, charged particle-induced DSBs in a given focus are most probably not independently processed, and/or they are processed with different velocities due to their different complexities. Both explanations stem from spatial correlation effects, but they involve different spatial scales: the first one is related to the presence of several DSBs within the same focus (therefore at Mbp distances) and the second one to complex DSBs due to local clustering of a DSB with other DNA lesions, including DSBs (involving distances of tens of bp) (*59*). The comparison between theoretical and experimental data show that at early times the repair is faster than that predicted by independent processing; this occurs also for the more realistic case where the foci have different complexities with an average number $\langle m \rangle$ of foci. This might be due to a repair mechanism in which the correlation in the processing of the foci inside a focus depends on their number, with a low number favoring correlated repair.

It is also possible to speculate on the relationship among different quantitative results at the cellular and molecular levels that have been presented in this work, focusing on

gamma rays and alpha particles. As shown in Table 2, the alpha-particle RBE values for cell killing and lethal mutations are 2.98 and 3.74, respectively. As for the RBE for DNA damage, the combination of experimental and simulation data presented above can provide an estimate on the number of DSBs per Gy produced by alpha particles. In fact, multiplying the average number of tracks per Gy, i.e., 8.8, as obtained by the dose-response curves (Fig. 7), by the average number of DSBs per track, i.e., 8, as obtained by the simulations, an average of 70.4 DSBs per Gy is found. Using the average value of 24.1 DSBs per Gy obtained from the gamma-ray dose-response curve, the RBE for DSB induction would be 2.92, a value very close to the RBE for cell killing. It is thus tempting to argue that the early surviving fraction depends mostly on the amount of the initial DNA damage. On the other hand, the RBE obtained for lethal mutation is significantly higher and possibly associated to a lesser degree with correctness in the repair of nonlethal damage. Concerning the repair kinetics, the experimental data fit well with the theoretical points at long postirradiation times only (see Fig 3). This is not consistent with the working hypothesis tested in the repair model, reported previously, that would require, if verified, an agreement also at short times. Therefore, our finding indicates that the damage complexity plays a more relevant role for the repair kinetics. The results for lethal mutations make it realistic to assume that the nonindependent processing of close damage is associated with a diminished correct repair capability of the alpha-particle-induced damage (*23, 60, 61*).

A difference, although less pronounced, also exists between the carbon ion RBE for cell killing and for lethal mutations, the values being 1.26 and 1.61, respectively (Table 2). However, for this radiation type, as emphasized earlier, a fraction of DSBs should be due to delta rays. For this reason we expect that the distribution of the number m of DSBs associated with a focus is rather heterogeneous, and a comparison between the RBE for initial damage and for cellular effects is expected to be more problematic.

In conclusion, although there are still pending problems in terms of quantification of clustered damage, the use of immunofluorescence techniques currently provides an important addition to the study of mechanisms associated with the radiation quality or LET dependence of biological effects of relatively low doses/fluences of charged particles. An integration of theoretical and computational tools may offer an additional approach direction for correlating cellular end points to the pattern of DNA damage.

APPENDIX

Here, we show the derivation of Eq. (1). We recall that the broken stick model used is generally made of a continuous approximation, and an expression is obtained for the probability of having DNA fragments of length x after a given dose has produced n DSBs on DNA molecules of length L. According to this description, if n DSBs are randomly induced on a DNA molecule of length L, then (i), the fragment probability distribution for the length x of the DNA fragments is (*45–47*):

$$P_n^L(x) = \frac{n}{L}\left(1 - \frac{x}{L}\right)^{n-1}, \tag{6}$$

and (ii), the broken stick distribution is obtained by making a weight average on n, where n follows a Poisson distribution with parameter $\lambda = DyM$ (where D is the radiation dose, y is the DSB yield and M is the chromosome mass) and it is given by (*48*):

$$f(m;M;Dy) = \left\{Dy[2 + Dy(M-m)]e^{-Dym}\right\}\chi(M) + \delta(M-m)e^{-DyM}. \tag{7}$$

We have therefore $f(m;M;Dy)\mathrm{d}M$ being the number of fragments with mass between m and $(m + \mathrm{d}m)$ after fragmentation induced by the dose D on a DNA molecule of mass M. $\chi(M)$ is the characteristic function of the segment $(0, M)$, which is 1 between 0 and M and 0 otherwise, and the last term with the Dirac delta function takes into account the probability of having an unbroken molecule. In going from Eq. (6) to Eq. (7) we have also substituted the lengths by the corresponding masses, i.e., $x \to m$, $L \to M$. To compute the average number of distinct foci we assume that DSBs at distances smaller than those corresponding to a given threshold mass M_1 cannot give rise to separate foci. We proceed in two steps: we first compute the average number of distinct foci when a given number n of DSBs are induced, making use of the distribution function in Eq. (1), and then we perform a Poisson weighted average.

Assume that n DSBs are randomly located on a chromosome with length L. The average number $\langle P\rangle_{x_1,n,L}$ of DSBs at a distance of at least x_1 ($x_1 < L$) with respect to the DSB to its left, or, in the case of the leftmost DSB, at distance at least x_1 with respect to the chromosome left edge, can be expressed by a recursive relation. In fact, it is easy to see that it obeys the following equation:

$$\langle P\rangle_{x_1,n,L} = \int_0^{x_1} dx \cdot P_n^L(x) \cdot \langle P\rangle_{x_1,n-1,L-x} + \int_{x_1}^{L} dx \cdot P_n^L(x) \cdot [1 + \langle P\rangle_{x_1,n-1,L-x}], \tag{8}$$

where $P_n^L(x)$ is the probability distribution given in Eq. (6). Putting together the first integral and the second term in the second integral, and performing the integration for the first term in the second integral, we arrive at:

$$\langle P\rangle_{x_1,n,L} = \int_0^{L} dx \cdot P_n^L(x) \cdot \langle P\rangle_{x_1,n-1,L-x} + \left(1 - \frac{x_1}{L}\right)^n, \tag{9}$$

where the integral can be extended up to $L - x_1$, since $\langle P\rangle_{x_1,n,L}$ is obviously zero for $x_1 > L$. The solution of this equation for generic $x_1 < L$ and n can be found by induction:

$$\langle P\rangle_{x_1,n,L} = n \cdot \left(1 - \frac{x_1}{L}\right)^n. \tag{10}$$

To obtain the average number $\langle s\rangle_{x_1,n,L}$ of distinct foci we have to consider that the first focus on the chromosome (ordering them from left to right) is detected even if its distance from the left chromosome edge is less than x_1. Therefore, $\langle s\rangle_{x_1,n,L}$ is obtained by adding to Eq. (10) the quantity:

$$\int_0^{x_1} dx \cdot P_n^L(x) = 1 - \left(1 - \frac{x_1}{L}\right)^n \tag{11}$$

Thus, the average number of distinct foci is:

$$\langle s\rangle_{x_1,n,L} = (n-1)\left(1 - \frac{x_1}{L}\right)^n + 1 \tag{12}$$

When $n = 1$ this expression is correctly equal to 1, since in this framework a single DSB induced by radiation is always associated to a single focus. The second step is the Poisson weighted average over n, with parameter $\lambda = DyM$, and with, similarly to what has been done before, the substitutions $x_1 \to M_1$ (and $L \to M$). Then, the average number of distinct foci $\langle s\rangle_{M_1,D,M}$, due to DSBs induced by a dose D on

a chromosome of length M and at distances greater than M_1, is given by:

$$\langle s\rangle_{M_1,D,M} = \sum_{n=1}^{\infty} e^{DyM}\frac{(DyM)^n}{n!}\langle s\rangle_{M_1,n,M} = [Dy(M-M_1)-1]e^{-DyM_1}+1, \quad (13)$$

which is Eq. (1).

ACKNOWLEDGMENTS

This work was partially supported by the National Institute of Nuclear Physics (INFN), TENORE experiment. The authors are indebted to Dr. R. Cherubini, the technical staff of Laboratori Nazionali di Legnaro and of Laboratori Nazionali del Sud of INFN, for the invaluable support during particle irradiation. The authors are also grateful to Dr. D. Alloni (University of Pavia, Italy) for fruitful discussions and communication of simulation data.

Received: July 5, 2014; accepted: January 16, 2015; published online: 00 00, 00

REFERENCES

1. Sachs RK, Chen AM, Brenner DJ. Review: proximity effects in the production of chromosome aberrations by ionizing radiation. Int J Radiat Biol 1997; 71:1–19.
2. Jackson SP, Bartek J. The DNA-damage response in human biology and disease. Nature 2009; 461:1071–78.
3. Rydberg B, Lobrich M, Cooper PK. Repair of clustered DNA damage caused by high LET radiation in human fibroblasts. Physica Medica 1998; 14 (Suppl 1):24–8.
4. Georgakilas AG, O'Neill P, Stewart RD. Induction and repair of clustered DNA lesions: What do we know so far? Radiat Res 2013; 180:100–9.
5. Prise KM, Pinto M, Newman HC, Michael BD. A review of studies of ionizing radiation-induced double-strand break clustering. Radiat Res 2001; 156:572–6.
6. Goodhead DT, Thacker J, Cox R. Effects of radiations of different qualities on cells: molecular mechanisms of damage and repair. Int J Radiat Biol 1996; 63:543–56.
7. Pinto M, Prise KM, Michael BD. Quantification of radiation induced DNA double-strand breaks in human fibroblasts by PFGE: testing the applicability of random breakage models. Int J Radiat Biol 2002; 78:375–88.
8. Belli M, Cherubini R, Dalla Vecchia M, Dini V, Esposito G, Moschini G, et al. DNA fragmentation in V79 cells irradiated with light ions as measured by pulsed-field gel electrophoresis. I. Experimental results. Int J Radiat Biol 2002; 78:475–82.
9. Bradley MO, Kohn KW. X-ray induced DNA double strand break production and repair in mammalian cells are measured by neutral filter elution. Nucleic Acids Research 1979; 7:793–804.
10. Olive PL. Impact of the comet assay in radiobiology. Mutat Res 2009; 681:13–23.
11. Prise KM, Ahnström G, Belli M, Carlsson J, Frankenberg D, Kiefer J, et al. A review of dsb induction data for varying quality radiations. Int J of Radiat Biol 1998; 74:173–84.
12. Lobrich M, Cooper PK, Rydberg B. Non-random distribution of DNA double-strand breaks induced by particle irradiation. Int J Radiat Biol 1996; 70:493–503.
13. Stenerlöw B, Hoglund E. Rejoining of double-stranded DNA-fragments studied in different size-intervals. Int J Radiat Biol 2002; 78:1–7.
14. Campa A, Alloni D, Antonelli F, Ballarini F, Belli M, Dini V, et al. DNA fragmentation induced in human fibroblasts by 56Fe ions: Experimental data and Monte Carlo simulations. Radiat Res 2009; 171:438–45.
15. Rogakou EP, Pilch DR, Orr AH, Ivanova VS, Bonner WM. DNA double-stranded breaks induce histone H2AX phosphorylation on serine 139. J Biol Chem 1998; 273:5858–68.
16. Rogakou EP, Boon C, Redon C, Bonner WM. Megabase chromatin domains involved in DNA double-strand breaks in vivo. J Cell Biol 1999; 146:905–16.
17. Sedelnikova OA, Rogakou EP, Panyutin IG, Bonner WM. Quantitative detection of ^{125}IdU-induced DNA double-strand breaks with γ-H2AX antibody. Radiat Res 2002; 158:486–92.
18. Asaithamby A, Uematsu N, Chatterjee A, Story MD, Burma S, Chen DJ. Repair of HZE-particle-induced DNA double-strand breaks in normal human fibroblasts. Radiat Res 2008; 169:437–46.
19. Rothkamm K, Lobrich M. Evidence for a lack of DNA double-strand break repair in human cells exposed to very low X-ray doses. PNAS 2003; 100:5057–62.
20. Boghal N, Jalali F, Bristow RG. Microscopic imaging of DNA repair foci in irradiated normal tissues. Int J Radiat Biol 2009; 85:732–46.
21. Leatherbarrow EL, Harper JV, Cucinotta FA, O'Neill P. Induction and quantification of γ-H2AX foci following low and high LET-irradiation. Int J Radiat Biol 2006; 82:111–8.
22. Antonelli F, Belli M, Cuttone G, Dini V, Esposito G, Simone G, et al. Induction and repair of DNA double-strand breaks in human cells: dephosphorylation of histone H2AX and its inhibition by calyculin A. Radiat Res 2005; 164:514–17.
23. Olive PL, Banath JP. Phosphorylation of histone H2AX as a measure of radiosensitivity. Int J Radiat Onc Biol Phys 2004; 58:331–5.
24. Paull TT, Rogakou EP, Yamazaki V, Kirchgessner CU, Gellert M, Bonner WM. A critical role for histone H2AX in recruitment of repair factors to nuclear foci after DNA damage. Curr Biol 2000; 10:886–95.
25. Karlsson KH, Stenerlöw B. Focus formation of DNA repair proteins in normal and repair-deficient cells irradiated with high-LET ions. Radiat Res 2004; 161:517–27.
26. Stucki M, Jackson SP. γH2AX and MDC1: Anchoring the DNA-damage-response machinery to broken chromosomes. DNA Repair 2006; 5:534–43.
27. Desai N, Davis E, O'Neill P, Durante M, Cucinotta FA, Wu H. Immunofluorescence detection of clustered γ-H2AX foci induced by HZE-particle radiation. Radiat Res 2005; 164:518–22.
28. Jakob B, Scholz M, Taucher-Scholz G. Biological imaging of heavy charged-particle tracks. Radiat Res 2003; 159:676–84.
29. Aten JA, Stap J, Krawczyk PM, van Oven CH, Hoebe RA, Essers J, et al. Dynamics of DNA double-strand breaks revealed by clustering of damaged chromosome domains. Science 2004; 303:92–5.
30. Jakob B, Splinter J, Durante M, Taucher-Scholz G. Live cell microscopy analysis of radiation-induced DNA double-strand break motion. PNAS 2009; 106:3172–7.
31. Costes SV, Boissiere A, Ravani S, Romano R, Parvin B, Barcellos-Hoff MH. Imaging features that discriminate between foci induced by high- and low-LET radiation in human fibroblasts. Radiat Res 2006; 165:505–15.
32. Belyaev IY. Radiation-induced DNA repair foci: spatio-temporal aspects of formation, application for assessment of radiosensitivity and biological dosimetry. Mutat Res 2010; 704:132–41.
33. Han J, Hendzel MJ, Allalunis-Turner J. Quantitative analysis reveals asynchronous and more than DSB-associated histone H2AX phosphorylation after exposure to ionizing radiation. Radiat Res 2006; 165:283–92.
34. Rothkamm K, Barnard S, Ainsbury EA, Al-Hafidh J, Barquinero JF, Lindholm C, et al. Manual versus automated γ-H2AX foci analysis across five European laboratories: Can this assay be used for rapid biodosimetry in a large scale radiation accident? Mutat Res 2013; 756:170–3.

35. Mah LJ, El-Osta A, Karagiannis TC. γ-H2AX: a sensitive molecular marker of DNA damage and repair. Leukemia 2010; 24:679–86.

36. Goodarzi AA, Jeggo PA. Irradiation induced foci (IRIF) as a biomarker for radiosensitivity. Mutat Res 2012; 736:39–47.

37. Suzuki M, Suzuki K, Kodama S, Watanabe M. Phosphorylated histone H2AX foci persist on rejoined mitotic chromosomes in normal human diploid cells exposed to ionizing radiation. Radiat Res 2006; 165:269–76.

38. Costes SV, Chiolo I, Pluth JM, Barcellos-Hoff MH, Jakob B. Spatiotemporal characterization of ionizing radiation induced DNA damage foci and their relation to chromatin organization. Mutat Res 2010; 704:78–87.

39. Yoshikawa T, Kashino G, Ono K, Watanabe M. Phosphorylated H2AX foci in tumor cells have no correlation with their radiation sensitivities. J Radiat Res 2009; 50:151–60.

40. Bewersdorf J, Bennett BT, Knight KL. H2AX chromatin structures and their response to DNA damage revealed by 4Pi microscopy. PNAS 2006; 103:18137–47.

41. Esposito G, Antonelli F, Belli M, Campa A, Simone G, Sorrentino E, et al. An alpha-particle irradiator for radiobiological research and its implementation for bystander effect studies. Radiat Res 2009; 172:632–42.

42. Belli M, Cherubini R, Galeazzi G, Mazzuccato S, Moschini G, Sapora O, et al. Proton irradiation facility for radiobiological studies at a 7 MeV Van de Graaff accelerator. Nucl Instrum Meth A 1987; 256:576–80.

43. Chang WP, Little JB. Evidence that DNA double-strand breaks initiate the phenotype of delayed reproductive death in Chinese hamster ovary cells. Radiat Res 1992; 131:53–9.

44. Suzuki K, Ojima M, Kodama S, Watanabe M. Radiation-induced DNA damage and delayed induced genomic instability. Oncogene 2003; 22:6988–93.

45. Montroll EW, Simha R. Theory of depolimerization of long chain molecules. J Chem Phys 1940; 8:721–7.

46. Litwin S. Distribution of radioactive recovery in randomly cut sediment DNA. J Applied Prob 1969; 6:275–84.

47. Van der Schans GP, Aten JBT, Blok J. Determination of molecular weight distribution of DNA by means of sedimentation in a sucrose gradient. Anal Biochem 1969; 32:14–30.

48. Cook VE, Mortimer RK. A quantitative model of DNA fragments generated by ionizing radiation, and possible experimental applications. Radiat Res 1991; 125:102–6.

49. Dini V, Antonelli F, Belli M, Campa A, Esposito G, Simone G, et al. Influence of PMMA shielding on DNA fragmentation induced in human fibroblasts by iron and titanium ions. Radiat Res 2005; 164:577–81.

50. Stenerlöw B, Carlsson KH, Cooper B, Rydberg B. Measurement of prompt DNA double strand breaks in mammalian cells without including heat-labile site: results for cells deficient for nonhomologous end joining. Radiat Res 2003; 159:502–10.

51. Rydberg B. Radiation-induced heat-labile sites that convert into DNA double-strand breaks. Radiat Res 2000; 153:805–12.

52. Alloni D, Campa A, Friedland W, Mariotti L, Ottolenghi A. Track structure, radiation quality and initial radiobiological events: Considerations based on the PARTRAC code experience. Int J Radiat Biol 2012; 88:77–86.

53. Chuykin IA, Lianguzova MS, Pospelova TV, Pospelov VA. Activation of DNA damage response signaling in mouse embryonic stem cells. Cell Cycle 2008; 7:2922–8.

54. Fernandez-Capetillo O, Celeste A, Nussenzweig A. Focusing on foci: H2AX and the recruitment of DNA-damage response factors. Cell Cycle 2003; 2:426–7.

55. van Attikum H, Gasser SM. Crosstalk between histone modifications during the DNA damage response. Trends Cell Biol 2009; 19:207–17.

56. Kinner A, Wu W, Staudt C, Iliakis G. γ-H2AX in recognition and signaling of DNA double-strand breaks in the context of chromatin. Nucleic Acid Res 2008; 36:5678–94.

57. Sedelnikova OA, Rogakou EP, Panyutin IG, Bonner WM. Quantitative detection of ^{125}IdU-induced DNA double strand breaks with g-H2AX antibody. Radiat Res 2002; 158:486–92.

58. Ponomarev AL, Costes SV, Cucinotta FA. Stochastic properties of radiation induced DSB: DSB distributions in large scale chromatin loops, the HPRT gene and within the visible volumes of DNA repair foci. Int J Radiat Biol 2008; 84:916–29.

59. Nikjoo H, O'Neill P, Terrissol M, Goodhead DT. Quantitative modelling of DNA damage using Monte Carlo track structure method. Radiat Environ Biophys 1999; 38:31–8.

60. Bracalente C, Ibañez IL, Molinari B, Palmieri M, Kreiner A, Valda A, et al. Induction and persistence of large γH2AX foci by high linear energy transfer radiation in DNA-dependent protein-kinase deficient cells. Int J Radiat Oncol Biol Phys 2013; 87:785–94.

61. Moore S, Stanley FKT, Goodarzi A. The repair of environmentally relevant DNA double strand breaks caused by high linear energy transfer irradiation – no simple task. DNA Repair 2014; 17:64–73.